Int J Adv Manuf Technol (2011) 55:921–933
DOI 10.1007/s00170-010-3123-3

ORIGINAL ARTICLE

The effect of high frequency and duty cycle in electrochemical microdrilling

M. A. H. Mithu · G. Fantoni · J. Ciampi

Received: 27 May 2010 / Accepted: 17 December 2010 / Published online: 12 January 2011

Abstract Pulse electrochemical micromachining possesses attractive features compared to conventional electrochemical machining processes based on a continuous current because it allows instantaneous electrochemical reaction by applying ultrashort voltage pulses. This study focuses on effects of applied frequency and duty cycle in electrochemical microdrilling on nickel plate. During microtool fabrication, tungsten micro-shafts are electrochemically etched to make two desired cylindrical microtools of different lengths and diameters to investigate the effects of pulsed frequency and duty cycle on electrochemical micromachining. The shape and size of the fabricated microholes, machining time, actual material removal rate (MRR_{act}) and the number of short circuits are considered as response factors. Shapes of micro-drilled holes are measured and compared to tool geometry. As for both short and long microtools, MRR_{act} and machining time respectively decreased and increased with an increase in applied frequency. But the MRR_{act} and machining time respectively increased and decreases with an increase in duty cycles. Experimental data reveals that there is a strong correlation among the shape and size of the microhole fabricated with applied frequency and duty cycle during microdrilling. However, MRR_{act} was found to be much higher for short tool than a long tool.

Keywords Electrochemical microdrilling · Short and long microtool · Nickel plate · Applied frequency · Duty cycle

M. A. H. Mithu (✉) · G. Fantoni · J. Ciampi
Department of Mechanical, Nuclear and Production Engineering,
University of Pisa,
56126 Pisa, Italy
e-mail: ah.mithu@ing.unipi.it

1 Introduction

The electrochemical micromachining (μECM) has become a promising area in the field of non-conventional machining processes, as it has a great potential on account of the versatility of its applications in the field of material removal processes. The basis of this process is electrolysis, which is governed by the laws established by Faraday. Two electrically conductive materials (workpiece and tool) are immersed into an electrolytic cell filled with an aquatic electrolyte, and on the application of an adequate potential difference between the electrodes, material removal takes place from the anode workpiece. By using high frequency short-pulse current, the electrochemical behavior inside the inter-electrode gap improves, and finally leads to improving surface finishing quality, efficiency and ensuring higher machining accuracy [1], therefore, finds majority of its applications in microhole drilling, shaping, deburring, etc. [2].

Mask-free electrochemical micromachining demonstrated impressive results by the use of ultrashort voltage pulses within narrower inter-electrode gaps. Therefore, sophisticated equipments are needed to handle the special conditions present during the μECM process that has yielded highly localized dissolution. Novel techniques, however, employ high-frequency pulsed voltage to reach better resolutions [3]. The applied voltage waveform plays a crucial role in defining a machining quality and surface finish of micro-machined part [4]. In the last decade, ultrashort voltage pulse has been studied by different researchers [5–7]. The effects of tool electrode size and insulation on μECM characteristics are also studied and found that the machining rate is significantly influenced by the tool electrode area for ultrashort pulses [8]. With the use of ultrahigh frequency inputs around gigahertz range,

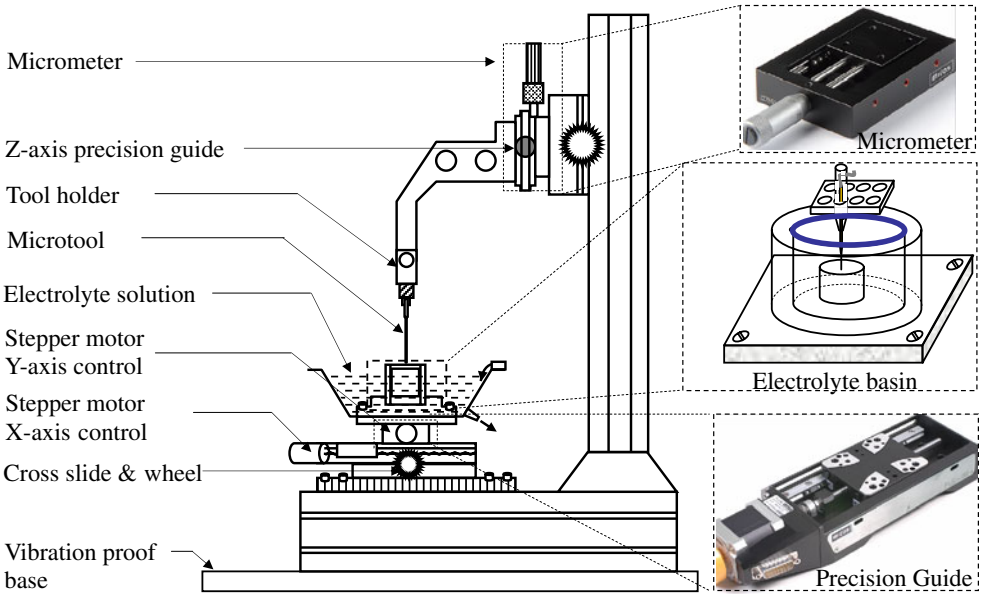

Fig. 1 Electrochemical micro-machining workcell

electrochemical reactions are restricted to electrode regions in close proximity which exceeds far beyond the 0.1 mm limited spatial resolution defined solely by electrolytic current density in dc voltages [5, 8]. Micromachining takes place during pulse-on time and pulse-off time is kept long enough to dissipate heated electrolyte and produced gas formed during pulse-on time. The microhole size increases as the pulse-on time and the applied voltage increase. However, the hole diameter converges to a certain size, and surface quality clearly worsens as the pulse duration increases. Moreover, if the pulse-off time is not long enough to remove the charged ions, the hole diameter increases continuously similar to the machining characteristics with dc voltage [9]. The influence of pulse-on/off ratio and voltage frequency on MRR has been studied [10]. Combined effect of ultrashort voltage pulses and voltage amplitude is also well studied [11, 12]. The material removal is decreased due to highly confined electron motion, which is a major problem in ultrashort-pulsed systems [13, 14] because ion migration takes the control due to transient current [15]. These electrical migration processes become dominant when the pulse duration is short. Thus, the relatively small inverse polarity is required on pulsed systems to promote the possible dissolution of plated product on the tool electrode during an inverse pulse [16]. But the machining time increases as the pulse frequency decreases [17]. On the other hand, with higher frequencies, the machined cavity diameter converges to the tool diameter.

Therefore, upon proper choice of the pulse duration, the dissolution of the workpiece material can be more strongly confined than in conventional electrochemical machining, where the reaction rates vary about linearly with the electrode separation [7]. From the aforestated literature review, it is found that with ultrashort voltage pulses, machining rate decreases with the increase of frequency. Machining accuracy also becomes poor as the pulse voltage and pulse-on time increases. Conversely, high off-time ultrashort pulses improve the localization of dissolution to sub-micrometer, therefore, for improving accuracy and surface finish, short-pulse voltage with high off-time is preferred. Moreover, tool dimension, i.e., the diameter of microtool has a significant

Table 1 Specifications of testing equipments used for electrochemical machining workcell

Test equipment	Specifications
Function generator	Keithley 3390 50 MHz; frequency resolution, 1μHz; amplitude, 10 mVpp–10 Vpp; 4 digits resolution; phase range, −360° to +360°; accuracy, 8 ns
Oscilloscope	Rigol DS1000E, 1 GHz, 2 channel, digital storage, 64 K color display
Linear travel guide	PLS-85, X and Y axes, maximum travel 155 mm, resolution of 0.1 μm, Uni-directional repeatability to 0.05 μm, maximum 100 mm/s, and,
	ML 40, Z-axis, maximum travel 40 mm, resolution of 0.1 μm, maximum 5 mm/s
Micro-controller	SMC corvus eco, 3-axes closed loop control, velocity <0.1 μm/s, 15–25 rev/s, linear interpolation, miCos GmbH

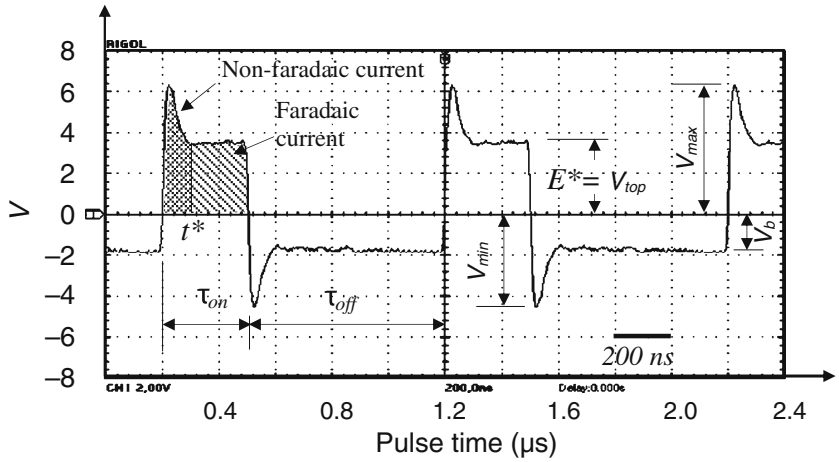

Fig. 2 Charging and discharging waveform during machining

effect in μECM using short pulses. This work is, therefore, carried out focusing on:

- effect of applied frequency on the shape and size of the fabricated microholes, machining time, and actual material removal rate (MRR_{act}) for long and short tool, and
- effect of duty cycle on machining time, MRR_{act}, the number of short circuits and shape and size of the fabricated microholes.

2 Experimental procedure

2.1 Experimental setup

The self-developed electrochemical micromachining workcell is shown in Fig. 1. It consists of an electrical function generator, an oscilloscope, computer-controlled guide system for feeding the tool and the workpiece. The guides were controlled by a 3-axes micro-step controller system that was interfaced with a desktop computer. The controller was controlled by customized software. The specifications of the testing equipments are given in Table 1. To avoid the physical contact between the tool (tungsten) and the workpiece (nickel plate), a tailored electronic circuit was used that automatically stopped and retracted the tool. After the set time, the circuit automatically restarted feeding the tool maintaining the predefined gap between the workpiece and tool. Moreover, the function generator, the oscilloscope, and the tailored circuit were used as signal source, signal analyzer, and tool feed controller, respectively, for in-process monitoring and controlling systems. Experiments were performed at room temperature. No circulation system was integrated during experimentation as μECM process involved negligible heat generation and the amount of precipitation was very small.

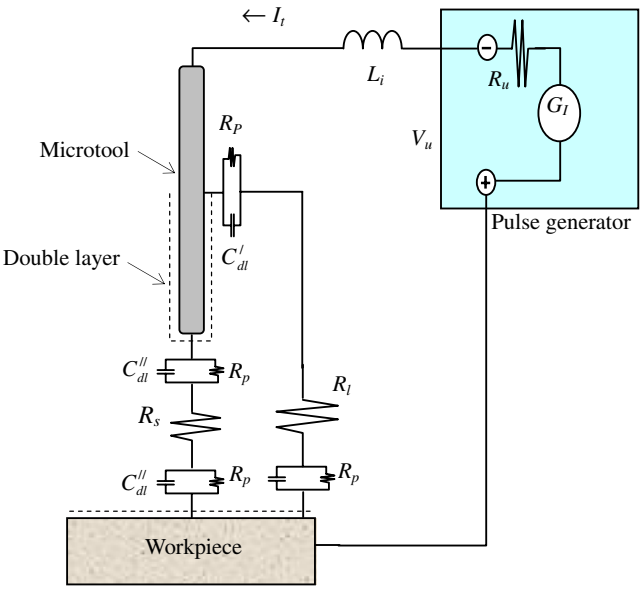

Fig. 3 Equivalent circuit model for electrical double layer potential

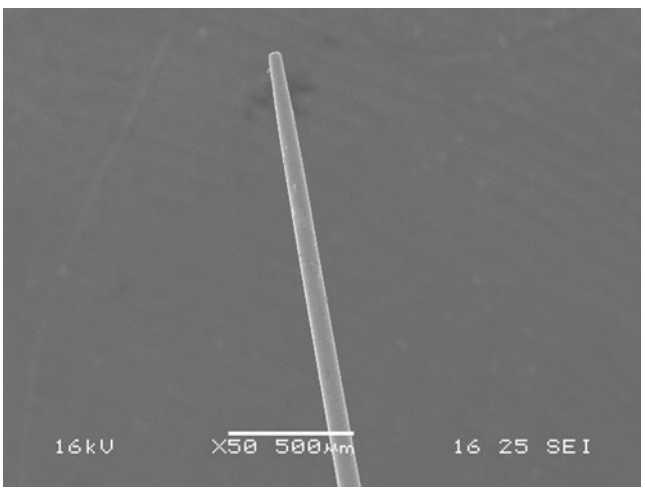

Fig. 4 SEM image of a fabricated long microtool

Table 2 Chemical composition and some basic physical properties of tungsten wire and nickel plate (source: Goodfellow catalog)

Physical properties	Tungsten tool		Nickel workpiece	
Chemical composition	99.9% W +		99.0% Ni +	
	Al	<50 ppm	Cu	<2,500 ppm
	Ca	<50 ppm	Fe	<4,000 ppm
	Cr	<50 ppm	Mg	<2,000 ppm
	Cu	<50 ppm	Mn	<3,500 ppm
	Fe	<50 ppm	Si	<1,500 ppm
	Mg	<50 ppm	Ti	<1,000 ppm
	Ni	<50 ppm	C	<1,500 ppm
	Si	<50 ppm	S	<100 ppm.
	Sn	<50 ppm.		
Poisson's ratio	0.28		0.312	
Yield strength (MPa)	550		660	
Tensile modulus (GPa)	411		199.5	
Electrical resistivity at 0–20°C (μOhm-cm)	5.4		6.9	
Coefficient of thermal expansion at 0–100°C (K^{-1})	4.5×10^{-6}		13.3×10^{-6}	
Thermal conductivity at 0–100°C ($Wm^{-1}\ K^{-1}$)	173		90.9	

ppm parts per million

2.2 Principle of material removal with pulsed voltage

The amount of material removed during μECM can be determined by combining Faraday's first law and Ohm's law [18] as stated in Eq. (1).

$$V_m = \frac{CEA}{gr}t \tag{1}$$

where, V_m=volume of material removed, C=the electrochemical constant, E=voltage value acquired by oscilloscope, A=electrode area, g=inter-electrode (tool-work) gap, r=electrolyte resistivity, t=time allowed for machining. For pulsed μECM, the volume of material removed for each voltage pulse is based on the assumption that material is removed only during the fraction of pulse-on time where faradaic current takes place, and flow rate is adequate to flush away the reaction products. Since the charging and discharging time depend on the constant resistor–capacitor (RC) circuit, material removal generally occurs in areas where electrolyte resistance is lower, i.e., where the tool-workpiece gap is very small [7, 19]. During every pulse period, the double layer is charged and discharged (i.e. created and destroyed) periodically over the two electrodes. The charging and discharging waveform attained during machining is shown in Fig. 2. As it is not simple to determine the faradaic current duration and its initial time, t^* (Fig. 2), a mathematical model has been proposed to calculate the material removal rate during the pulse-on time with a good approximation [20].

Considering that in the etching process, material removal takes place only for all pulse-on time durations; the volume of material removed ($V_{\text{m-on time}}$) could be obtained from,

$$V_{\text{m}-\text{ontime}} = \int_0^{\tau_{\text{on}}} \frac{CEA}{gr}dt, \tag{2}$$

where, τ_{on} is pulse-on time during each pulsed period.

Since the material removal acts only during the time corresponding to faradaic-currents, the integral has to be rearranged accordingly for better approximation as follows:

$$V_{\text{on}-\text{time}} = \int_{t^*}^{\tau_{\text{on}}} \frac{CEA}{gr}dt = \int_{t^*}^{\tau_{\text{on}}} \left[\int_s \frac{CA}{gr}Eds\right]dt$$
$$= CE^* \int_{t^*}^{\tau_{\text{on}}} \left(\frac{\overline{S}}{\overline{g}.\overline{r}}\right)dt = \frac{C\overline{S}E^*}{\overline{g}\ \overline{r}}\left(\tau_{\text{on}} - t^*\right), \tag{3}$$

Table 3 Machining conditions for microhole fabrication

Factors	Parameters/value	
Working materials	Tool material	Tungsten microtool
	Work material	Nickel plate, 50×50×0.075 mm
Electrolyte conc. (M/L)	0.2 M HCl solution (without circulation)	
Electrical parameters	Frequency	0.5–8 MHz
	Duty cycle	15–40%
	V_{pp}	16.1 V
	V_{max}	10.6 V
	V_b	−5.0 V
Tool feed	0.05 to 0.8 μm/s, computer controlled	

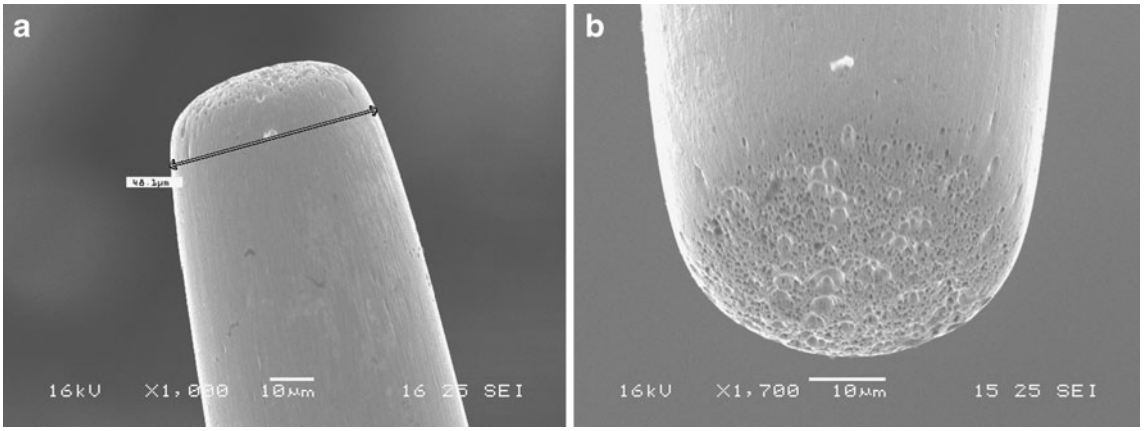

Fig. 5 A large-scale image of a long microtool tip **a** before and **b** after machining

where, S is the surface immersed into electrolyte, t^* is the start time of the flat voltage and E^* is the flat voltage from t^* to τ_{on} and $\overline{S}$, $\overline{g}$, $\overline{r}$ are the average values of S, g, and r, respectively, coming from the surface integral. The values of g and r vary along the surface and have a minimum value in the closer part of the tip that supplies the higher contribution to the surface integral.

Again, τ_p is the time taken for one complete oscillation and δ_τ is the fraction of τ_p, called duty cycle in percentage and γ^* is the percentage of pulse-on time to start almost-flat voltage (median value of E becomes almost-flat voltage) and is measured with the aid of a digital oscilloscope. Putting these in Eq. 3,

$$V_{\text{on-time}} = \frac{C\overline{S}E^*}{\overline{g}\,\overline{r}}\delta_\tau\left(1-\gamma^*\right)\tau_p = \frac{C\overline{S}E^*}{\overline{g}\,\overline{r}f}\delta_\tau\left(1-\gamma^*\right), \quad (4)$$

where, f is the applied frequency in hertz (cycles per second). However, this approximation by excess of MRR was calculated as

$$\text{MRR} \cong \frac{V_{\text{on-time}}}{\tau_{\text{on}}+\tau_{\text{off}}} = \frac{V_{\text{on-time}}}{\tau_p}, \quad (5)$$

where, $V_{\text{on-time}}$ is the volume of material removed for one pulse-on time.

Thus, applying ultrashort pulses between tool electrode and workpiece, faradaic dissolution current flows only in the very confined region [17]. The inductance prevents instantaneous reversal of the current, while an appropriate value of negative voltage applied to the workpiece during the pulse-off time accelerates the creation of the double layer without the dissolution of the tool. While the pulse duration of machining current is shortened to a few nanoseconds, the electrochemical process cannot achieve

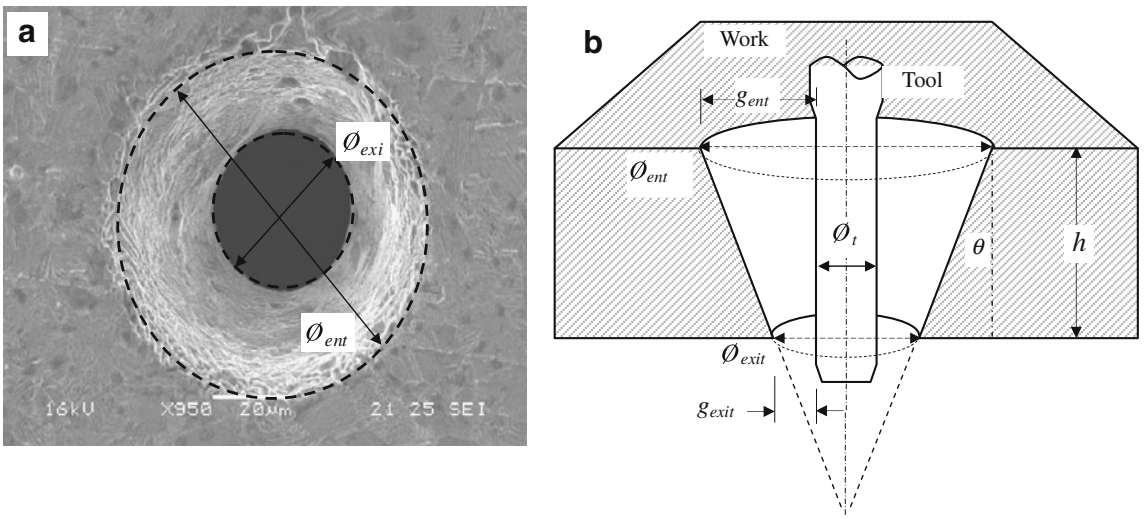

Fig. 6 **a** SEM image and **b** schematic illustration of the fabricated microhole

stationary condition owing to the extremely short-pulse duration [21]. Electrolyte resistance, inductance, and electrical double layer provide an equivalent RCL circuit in electrochemical cell is shown in Fig. 3, where, C_{dl}, is the capacitance of the double layer, which is nothing but a parallel-plate capacitor with high capacity, R_P, is polarization resistance of the double layer, R_s is short path resistance and R_l is long path resistance of the equivalent circuit, L_i is the inductance of the electric wires, R_u is the internal resistance of the pulse supplier, V_u is the exit tension of the pulse supplier, I_t is the total current, and G_I is the ideal pulse supplier.

2.3 Fabrication of microtools and microholes

The μECM needs a tool electrode on micron scale including high electric and thermal conductivity, corrosion resistance, stiffness to withstand the pressure of electrolyte and mechanical strength. While a wide choice of noble metals is available, tungsten and its alloy, platinum and its alloy, some super alloys are widely used [22]. In this experiment, straight tungsten wire (Goodfellow Ltd., UK) of 0.38 mm in diameter, 0.5 m in length was used to fabricate microtools. The required tungsten piece was cut from as supplied long wire and the ends of the specimen were ground, polished, and cleaned. The length and tool tip condition were also checked under optical microscope before etching to ensure nonexistence of flaw/crack. During microtool fabrication, the electrolyte must be capable of dissolving tungsten wire to give it a desired shape. In this context, solution of KOH was able to serve the purpose of dissolving the material like tungsten. In the fabrication of microtool, KOH electrolytes with concentration of 0.08–1.4 M were prepared with fresh deionized water. The specimen was fixed to a holder unit and immersed vertically at a constant depth into the electrolytes basin containing caustic solution of specific concentration. On the application of a potential difference between electrodes, the dissolution process proceeded and a certain etching time resulted in a straight micro-shaft with a certain diameter.

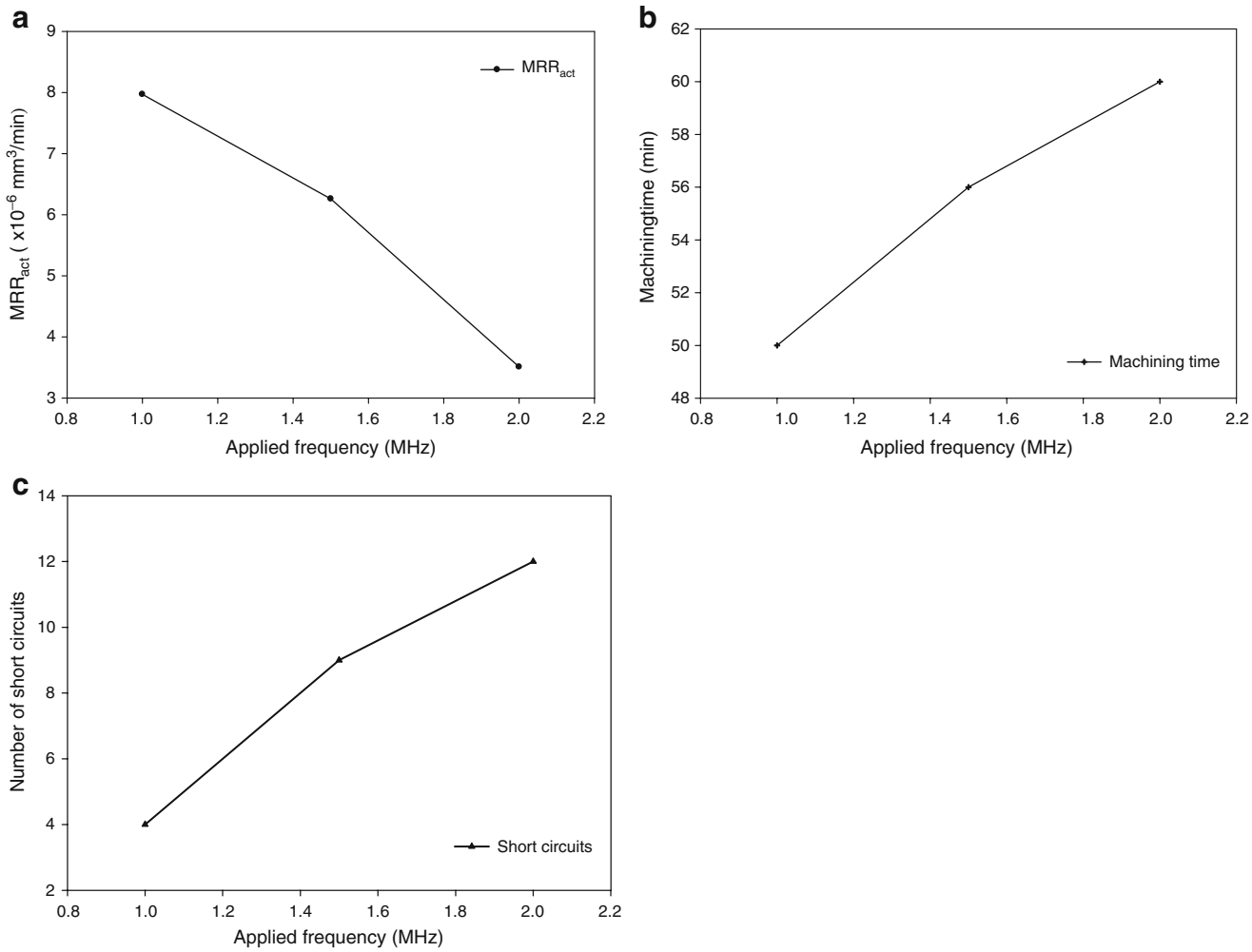

Fig. 7 Effect of applied frequency on **a** MRR$_{act}$, **b** machining time, and **c** number of short circuits occurred during machining for a long microtool

Each of the tools was rinsed in the hot water to remove foreign particles and the formed oxides, and the diameter of the tool was measured under optical microscope and scanning electron microscope (SEM). A typical microtool fabricated is shown in Fig. 4.

Besides, the selection of workpiece material was based on the properties of corrosion and heat resistance. Nickel, being inert against most chemicals, is a metal commonly applied in microtechnology [23]. An uncoated nickel plate of 50×50×0.075 mm in dimension (Goodfellow Ltd., UK) was selected as work material. Less toxic and dilute electrolyte, 0.2 M HCl was selected during microholes fabrication. Hence, the acidic electrolyte allowed refreshing electrolyte in the machining area easily because the acid electrolyte usually produced by-product much less than common salt electrolytes [24–26]. Fresh and clean electrolytes were used with a view to reduce the effects associated with the precipitation. This experiment was performed at room temperature and no electrolyte circulation system was integrated as the process involved negligible amount of heat generation and precipitation formation. The chemical composition and some basic physical properties of tungsten wire and nickel plate are summarized in Table 2.

During the fabrication of microtools, the tungsten specimens were fixed with the holder unit, positioned vertically downward, and fed through the circular cathode that was immersed into the KOH electrolytes basin. The feeding was controlled by the servo-controlled feed mechanism of Z stage. But during microdrilling, the fabricated microtools were fixed with the tool holder unit, and then tool was fed towards the nickel workpiece. Microtool feeding was controlled by the servo-controlled feed mechanism of Z stage, while the workpiece was positioned horizontally by X–Y axes travel guides, if required. The, machining conditions applied in microdrilling process are summarized in Table 3. The dimension of fabricated microholes, material removal rate, machining time, and the frequencies of short circuits were recorded and taken into account as response factors.

2.4 Measurements

Image analysis application software, Easy Analysis, integrated with the optical microscope (Nikon SMZ800) was used to measure the diameter and length of the tool produced by μECM. Entrance and exit diameters of each fabricated microhole were also measured using the same microscope. In addition, SEM was used to acquire clear

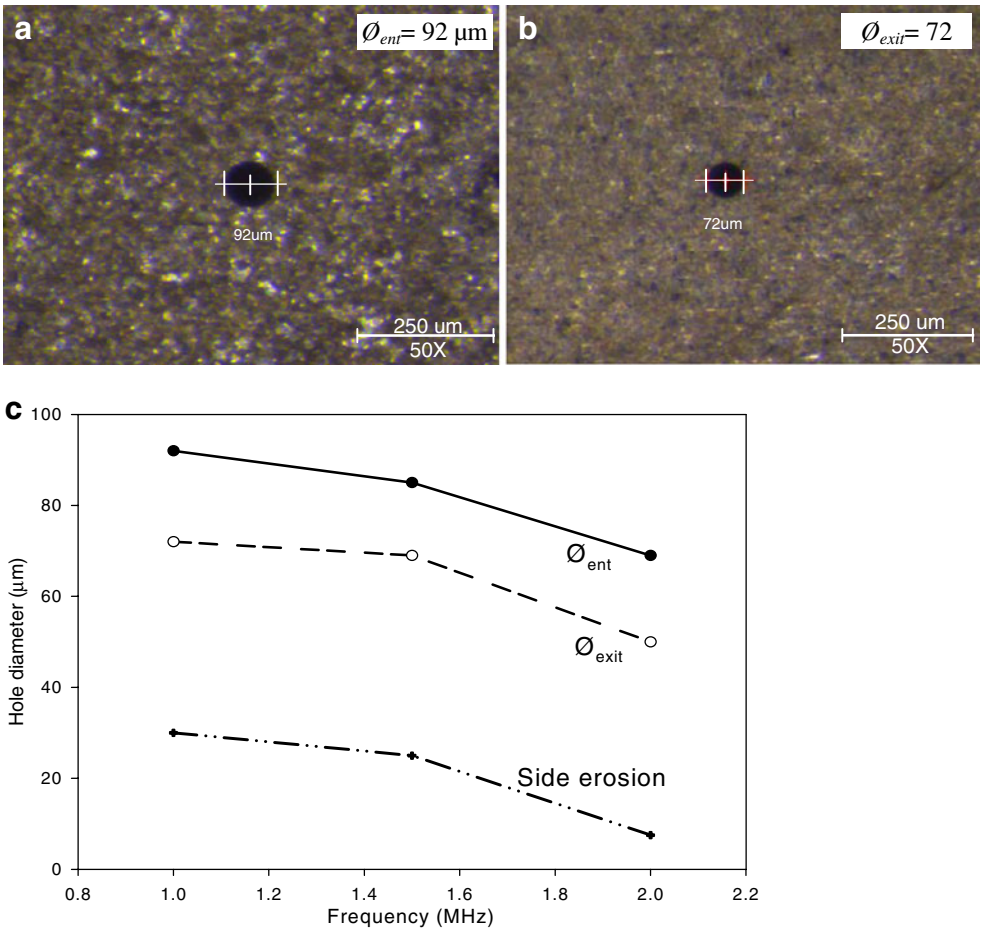

Fig. 8 Microscopic image of **a** entrance and **b** exit of the same microhole, and **c** variation in side erosions for different frequencies

picture of the fabricated microtool and the tool tip, are illustrated in Fig. 5.

Although the tool electrodes were cylindrical, the entrance and exit diameter of the machined microhole were not same due to: (1) shape restriction, (2) etching process in case of non-insulated tool, and (3) corner etch of the hole entrance in addition with the linear etching, and the result is the tapering of the side wall. Therefore, to evaluate the total material removed during machining, both entrance and exit diameters were measured. The amount of material removed from the workpiece can be calculated from the truncated cone Eq. (6).

$$V_m = \frac{\pi h}{12}\left(\phi_{\text{ent}}^2 + \phi_{\text{ent}}.\phi_{\text{exit}} + \phi_{\text{exit}}^2\right) \tag{6}$$

where, $\varnothing_{\text{ent}}$, $\varnothing_{\text{exit}}$, h were hole entrance diameter, hole exit diameter and thickness of the metal plate, respectively, shown in Fig. 6, where, g_{ent}, g_{exit}, $\varnothing_t$ are side gap at the entrance and exit of the microhole, microtool diameter. The MRR_{act} is calculated as the total volume of material removed from the workpiece over the total machining time which is expressed as cube millimeter per minute.

3 Experimental results and discussion

This experimental scheme is focused on observations related to the effects of applied frequency and duty cycle used in μECM process. To do this, microtools are classified into two groups: short tool and long tool are smaller than 1,500 μm and minimum length of 1,500 μm, respectively.

3.1 Effect of applied frequency

A 52-μm mean diameter tool of length 3,700 μm has been positioned above the workpiece in a vertical etch position, and allowed to machine on nickel plate. During this experiment, only the applied frequencies were varied while other parameters were kept constant. Figure 7 exhibits the influence of applied frequency on MRR_{act}, machining time

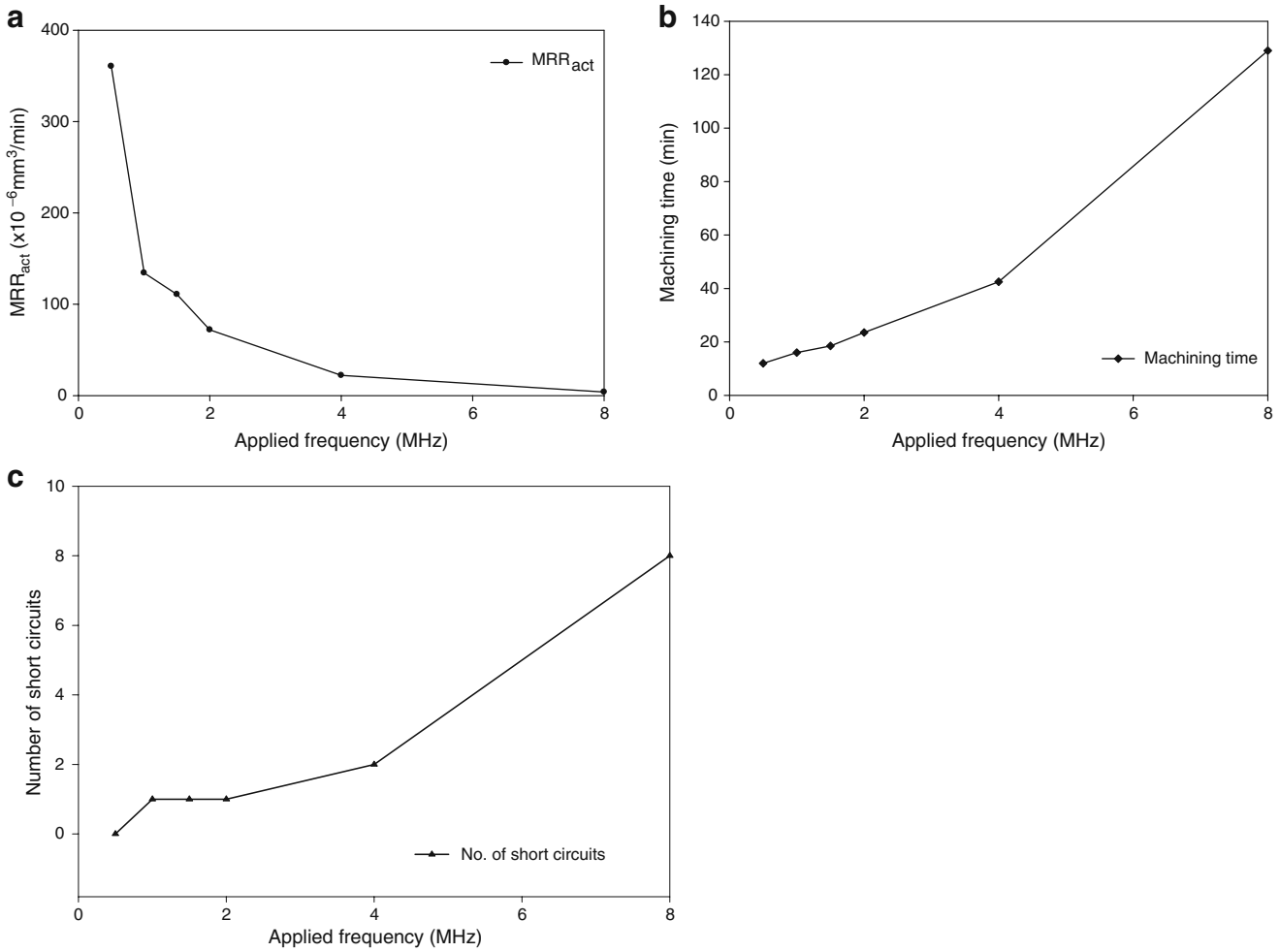

Fig. 9 Effect of applied frequency on **a** MRR_{act}, **b** machining time, and **c** number of short circuits for short microtool

and the number of short circuits occurred during micro-drilling processes. From Fig. 7a–b, it is evident that MRR_{act} decreases and the machining time increases with an increase in electrical frequency where the pulse-on/off ratio of 1:2.3. This is can be attributed to decrease in MRR_{act} with the increase in applied frequency.

Minimum pulse-on time needed to overcome the effects associated with double layer capacitor is found to be in the range of 10~30 ns for the electrodes with the diameter ranging 40~80 μm in diameter [8]. In this work, the applied pulse-on time is fixed to 300 ns (30% duty cycle) which is much higher than the required ultrashort voltage pulses. Consequently, effect of non-transient current becomes negligible and Faradaic current dominates the material dissolution process. As the applied frequency increases, the electrical double layer capacitance decreases and electrolytic resistance increases. The increased electrolytic resistance causes increased cell impedance, which in turn, decreases the current density into the electrolyte. Therefore, the amount of Faradaic current decreases with the increase in applied frequency and causes gradual decrease in MRR_{act} and increase in machining time.

It is also observed that the number of short circuits increases with the applied frequency. With the increasing frequency, the tool electrode fails to maintain a constant gap during machining for the same feed rate and results in increased number of short circuits. On the other hand, when high frequency is applied, entrance and exit diameters are found to be smaller. This is due to the less amount of side erosion that occurs during machining resulting in reduction of entrance and exit of hole diameter, which is also found in a similar work [13]. The entrance and exit of fabricated microholes, and the corresponding side erosions for different applied frequencies are shown in Fig. 8.

Again, a microtool with 76 μm in diameter and 690 μm in length was selected and then machining was carried out keeping all other parameters fixed. Figure 9 exhibits the influence of frequency on MRR_{act} and machining time in microdrilling processes. From the figures, it is clear that MRR_{act} and the machining time also respectively decreases and increases with an increase in applied frequency. However, it is also observed that for the same range of pulse-on time, actual MRR is found to be much higher for the lower applied frequency for a short tool. This is due to the combined effect of tool diameter

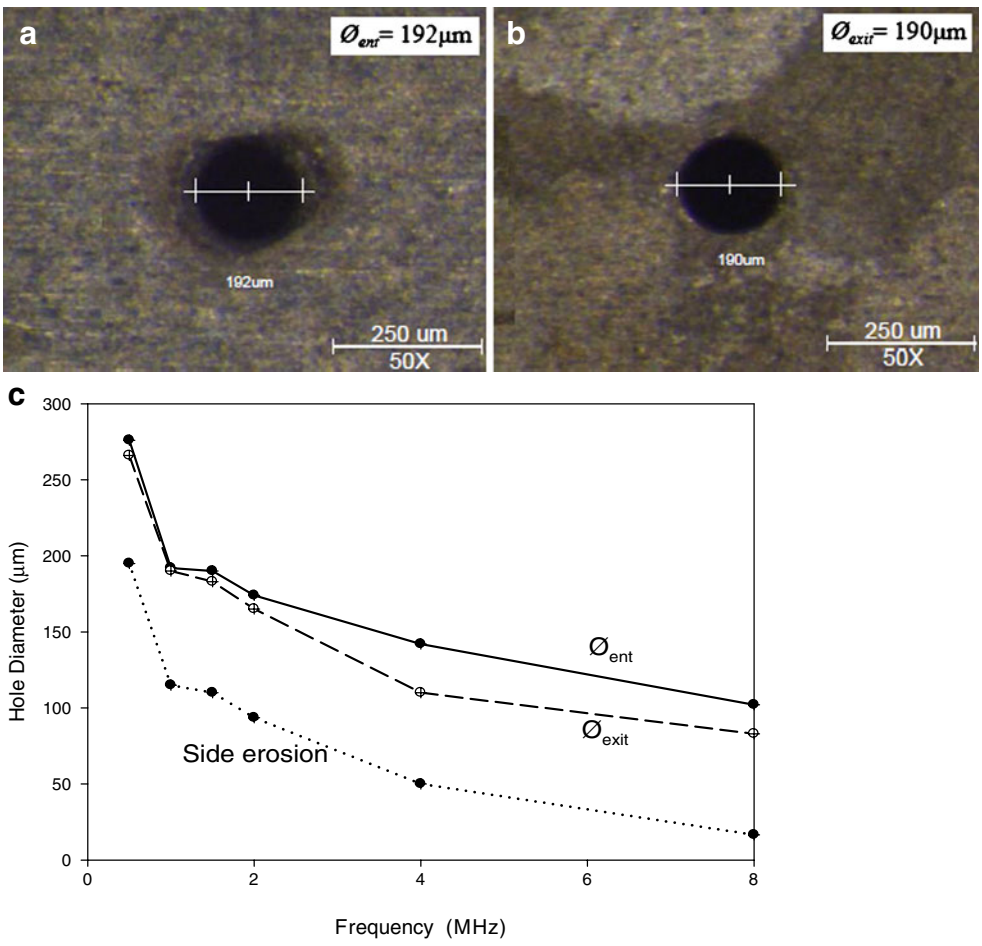

Fig. 10 **a** Entrance and **b** exit diameter of the hole fabricated at 1 MHz, and **c** entrance and exit diameters of microholes and side erosions for various applied frequencies

and length of the tool used as the actual MRR increases and decreases with the increase in tool diameter [8] and tool length, respectively.

Again, from Fig. 9c, it is found that no short circuit occurs for applied frequency of 0.5 MHz even at a very high feed rate ranging from 0.2 to 0.8 μm/s. This is because MRR increases rapidly with decreasing applied frequency or a high pulse-on time, as shown in Fig. 9a. Moreover, gradual decrease and increase in actual MRR and machining time, respectively, are observed with increase in frequency ranging from 2 to 8 MHz. Though hole diameter can be controlled precisely for frequency of 8 MHz, requirement for higher machining time and frequent occurrence of short circuits at this applied frequency make it inappropriate for micromachining.

This observation can be explained in accordance with the Ohm's law. The time constant τ for charging the double layers is the product of electrolyte resistance and double layer capacitance, C_{dl}. Because of the shorter tool, short path resistance R_s is smaller than the long path resistance R_l and the double layer charging time constant τ_s of the shorter path is relatively small compared to charging time constant for long path τ_l. On the other hand, time constant τ_l of the longer path is bigger than τ_s due to the larger electrolyte resistance, R_l. Again, faradaic current decreases with the increase in tool length. As a consequence of this reduction in faradaic current, the material removal rate decreases proportionately to the rate of increase in electrolyte resistance. As for short tool length, the machinable area is restricted to the adjacent region of the tool as the electric current flows through the shorter path with the electrolyte resistance R_s. However, for long tool, the dissolution of material takes place over a large space from the surface of anode material producing a small hole as the dispersed materials cannot be measured during machining. The microholes fabricated on the plate are found almost straight up to a certain limit of applied frequency of 1.0 MHz and after that limit, conicity of the hole increases with the increase applied frequency, as illustrated in Fig. 10.

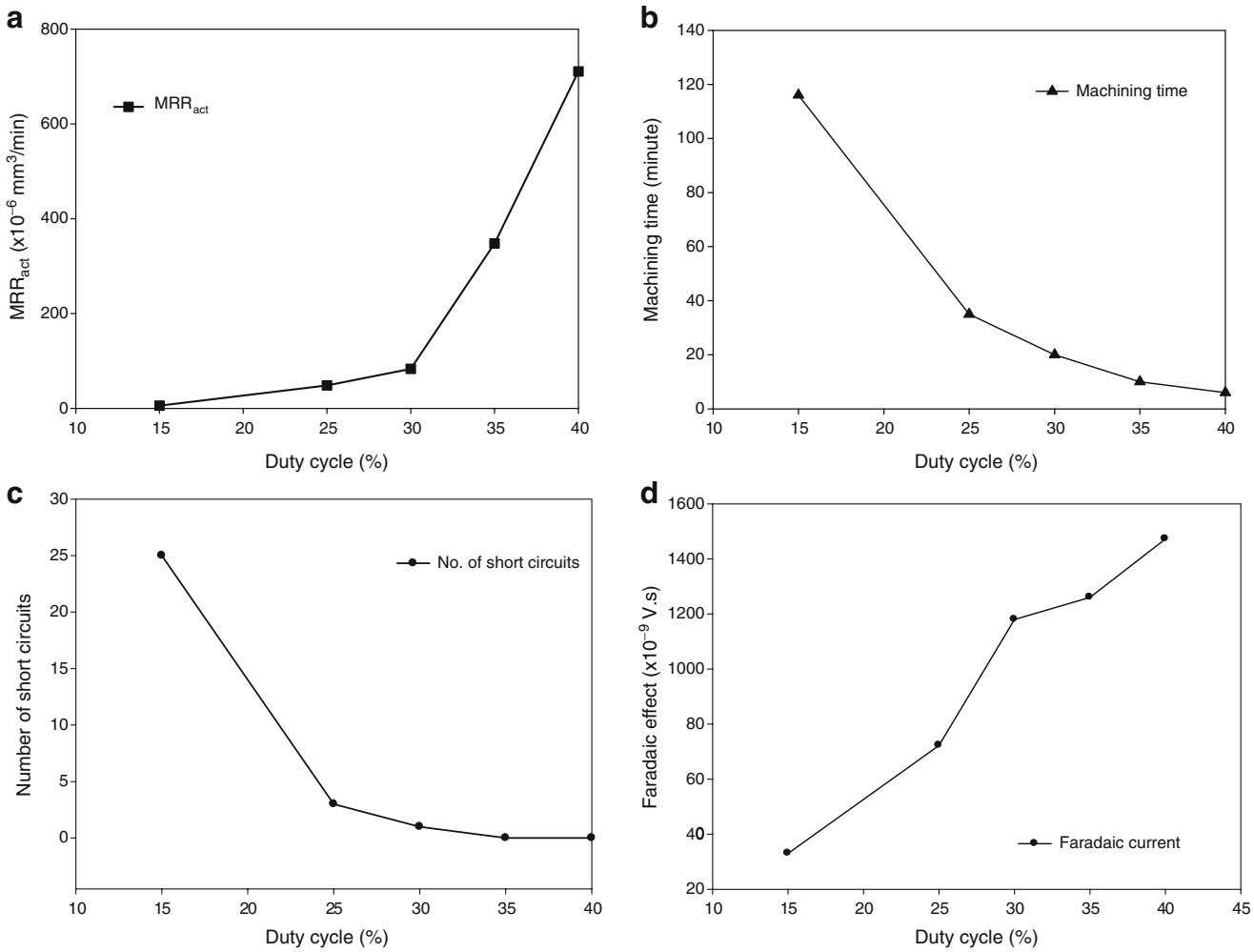

Fig. 11 Effect of duty cycle on **a** MRR$_{act}$, **b** machining time, **c** number of short circuits, and **d** amount of faradaic effect for short microtool

3.2 Effect of duty cycle

Together the on-time (τ_{on}) and off-time (τ_{off}) pulses comprise a single cycle, and duty cycle is the ratio of pulse-on time and total cycle time. As the frequency determines the pulse period, this section describes the effect of duty cycle with applied frequency during micro-drilling on nickel plate. The prefabricated short microtool (L=690 μm) was employed for this study and the machining carried out keeping the other parameters fixed. Figure 11 exhibit the influence of duty cycle on MRR_{act}, machining time, frequencies of short circuit occurrences and amount of faradaic effect ($V_{top} \times (\tau_{on} - t^*)$) during microdrilling processes. From these figures, it is found that MRR_{act} and the machining time respectively increases and decreases with an increase in duty cycle. However, for the same applied frequency, MRR_{act} is found to be much higher for high percentage of pulse-on time.

From Fig. 11c–d, it is found that no short circuit occurs for higher duty cycles even for a high feed rate ranging from 0.3 to 0.4 μm/s. This is due to rapid increase in material removal rate with increasing duty cycles for the same applied frequency of 1.0 MHz. Consequently, as shown in Fig. 11b rapid decrease in machining time are observed with increase in duty cycle. Thus the diameter of the hole cannot be controlled precisely for higher duty cycles as the side erosion rapidly increases for the higher duty cycles and their corresponding machining times are very low compared to the lowest duty cycle applied in this study. In Figure 12a–c, illustrating the diameters of the holes fabricated on the nickel plate for numerous applied duty cycles, it is found that the microhole diameter is small for lower duty cycles applied and gradually increases with an increase in duty cycle. This can be attributed to the lower and higher side erosions for lower and higher applied duty cycles, respectively.

The effect of duty cycle for applied frequencies can be explained by the existence of the faradaic effect created during microdrilling processes. Referring to Eqs. (3) and (4), volume of material removed is proportional to the product of the almost-flat voltage value acquired by oscilloscope ($E^* = V_{top}$) and time for remaining the voltage value at this level. When the small tool was used, both the voltage values acquired by the oscilloscope (E^*) and time to remain the voltage value on the same level, ($\tau_{on} - t^*$) gradually increased with the increase in the duty cycle.

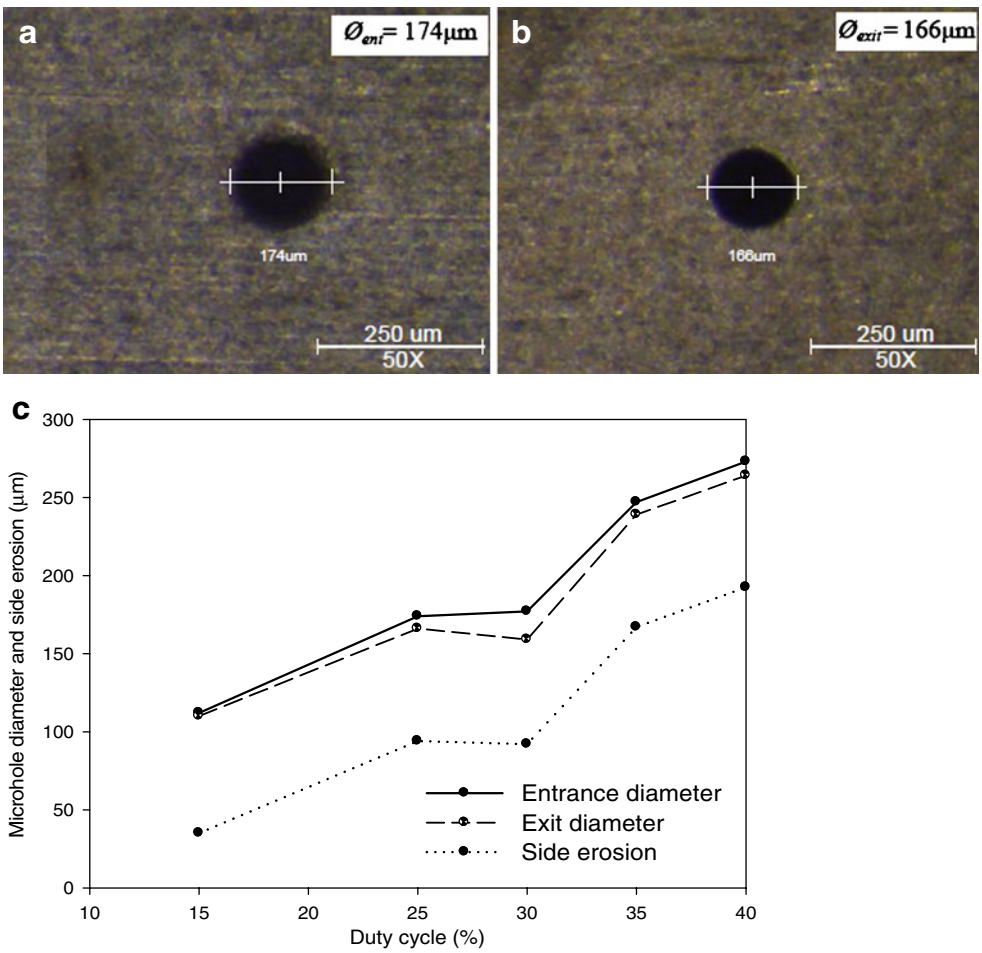

Fig. 12 **a** Entrance and **b** exit diameters of the holes for duty cycle of 25%, and **c** microhole diameters and corresponding side erosions for different duty cycles

Therefore, the product of voltage value and the corresponding time determining the faradaic effect increases rapidly with increase of the duty cycle and results in rapid dissolution of material during machining. It was found that the material removal rate increases drastically for the applied duty cycle set to 30% and above. At this value of applied duty cycle, material dissolution was so high that no short circuit occurs even at a feed rate of 0.4 μm/s. As a consequence, the side gap increases very rapidly and it was not possible to control the diameter of the microhole.

To perform micromachining effectively, microtool feed rate should have a linear relationship with the material removal rate. Therefore, the feed rate needs to be adjusted with MRR, which effects on the machining time. In microdrilling, the inter-electrode gap should be maintained very small and narrow for achieving higher machining accuracy in the micromachining domain. When the applied duty cycle was reduced to a value less than 30%, a sudden jump in the current density occurred, that could be monitored with the oscilloscope. This phenomenon indicates that possible corrective action requires for preventing the microtool from the possibilities of micro-sparks when the tool approaches to the workpiece. Therefore, the control system with feedback mechanism that controls the tool feeding system is used in the microdrilling process. If the tool electrode is in contact with the workpiece, the system automatically feeds backward until the tool gets detached and this attempt continues until a stable current density is achieved.

4 Conclusion

As a result of the analysis and experiments conducted for both applied frequency and duty cycles in electrochemical microdrilling, important conclusions are observed as follows:

- The MRR and machining time decreases and increases, respectively, with the increase in applied frequency for both the long and short microtool for a particular combination of micromachining parameters.
- The number of short circuits also increases with the increase of applied frequency. The entrance and exit diameters are found to be smaller because of less amount of side erosion.
- For the same range of pulse-on time and applied frequency, the MRR_{act} is much higher and machining time is smaller for the short tool as compared to long tool.
- The entrance and exit diameters of the hole fabricated on the nickel plate are found smaller for long microtool but the conicity of the hole increases with the increase in applied frequency.
- The MRR_{act} increases and the machining time decreases with an increase in duty cycle. No short circuit occurs for higher duty cycles even at a very high feed rate used for μECM.
- For higher duty cycles, the microhole diameters cannot be controlled precisely as the side erosion increases rapidly and the machining time is very low compared to lower duty cycles.

Acknowledgement This research work has been carried out in the Department of Mechanical, Nuclear and Production Engineering and funded by Ministero dell'Istruzione dell'Università e della ricerca, Programmi di ricerca cofinanziati (COFIN), Italia. Authors are deeply indebt to Prof. M. Santochi and Prof. G. Tantussi for cordial supervision and valuable advice. Authors also acknowledge to MMA Khan, DIMNP for his assistance while writing the article. Technical staffs of the DIMNP are also acknowledged.

References

1. Burkert St, Schulze H-P, Gmelin Th, Leone M (2009) The pulse electrochemical micromachining (PECMM)—specifications of the pulse units. Int J Mater Form 2(1):645–648. doi:10.1007/s12289-009-0464-2
2. Sen M, Shan HS (2005) A review of electrochemical macro- to micro-hole drilling processes. Int J Mach Tools Manuf 45(2):137–152. doi:10.1016/j.ijmachtools.2004.08.005
3. Hung W, Sundarram S, Ozkeskin F, Powers M, Manriquez J, Vasiraju V (2009) Electrochemical micro machining: A case study for synergistic international industry-academia collaboration, American Society for Engineering Education, AC 2009-2502 Past ASEE Annual Conferences & Expositions, June 14 – 17, 2009, Austin, TX http://www.meteconline.org/view_abstract.php?id=1948 Accessed 22 Nov 2010
4. Ahn SH, Ryu SH, Choi DK, Chu CN (2004) Electro-chemical micro drilling using ultra short pulses. Precis Eng 28:129–134. doi:10.1016/j.precisioneng.2003.07.004
5. Schuster R, Kirchner V, Allongue P, Ertl G (2000) Electrochemical micromachining. Science 289(5476):98–101. doi:10.1126/science.289.5476.98
6. Bhattacharyya B, Munda J (2003) Experimental investigation into electrochemical micromachining (EMM) process. J Mater Process Technol 140:287–291. doi:10.1016/S0924-0136(03)00722-2
7. Kock M, Kirchner V, Schuster R (2003) Electrochemical micromachining with ultrashort voltage pulses—a versatile method with lithographical precision. Electrochim Acta 48:3213–3219. doi:10.1016/S0013-4686(03)00374-8
8. Park BJ, Kim BH, Chu CN (2006) The effects of tool electrode size on characteristics of micro electrochemical machining. CIRP Annals-Manuf Technol 55(1):197–200. doi:10.1016/S0007-8506(07)60397-7
9. Wang J-J J, Chung CK, Wu BH, Liao YY (2007) Fabrication of wedge-shape tool via electrochemical micromachining with diamond-like carbon coating. J Mater Process Technol 187–188:264–269. doi:10.1016/j.jmatprotec.2006.11.069
10. Munda J, Bhattacharyya B (2008) Investigation into electrochemical micromachining (EMM) through response surface methodology based approach. Int J Adv Manuf Technol 35:821–832. doi:10.1007/s00170-006-0759-0
11. Cagnon L, Kirchner V, Kock M, Schuster R, Ertl G, Gmelin WT, Kück H (2003) Electrochemical micromachining of stainless steel

by ultrashort voltage pulses. Z Phys Chem 217:299–313. doi:10.1524/zpch.217.4.299.20383
12. Jo CH, Kim BH, Chu CN (2009) Micro electrochemical machining for complex internal micro features. CIRP Annals-Manuf Technol 58:181–184. doi:10.1016/j.cirp.2009.03.072
13. Davydov AD, Volgin VM, Lyubimov VV (2004) Electrochemical machining of metals: fundamentals of electrochemical shaping. Russ J Electrochem 40(12):1230–1265. doi:10.1007/s11175-005-0045-8
14. Kenney JA, Hwang GS (2005) Electrochemical machining with ultrashort voltage pulses: modelling of charging dynamics and feature profile evolution. Nanotechnology 16:S309–S313. doi:10.1088/0957-4484/16/7/001
15. Luo YF (2006) Differential equations for the ultra-fast transient migration in electrolytic dissolution. Electrochem Commun 8:353–358. doi:10.1016/j.elecom.2005.11.028
16. Uhlmann E, Doll U, Forster R, Schikofsky R (2001) High precision manufacturing using PEM. Proc. of the International Symposium for Electromachining (ISEM XIII), Bilbao, Spain (vol. 1):261–268
17. Ryu SH (2009) Micro fabrication by electrochemical process in citric acid electrolyte. J Mater Process Technol 209:2831–2837. doi:10.1016/j.jmatprotec.2008.06.044
18. McGeough JA (1988) Advanced methods of machining. Chapman and Hall Ltd, London
19. Bhattacharyya B, Mitra S, Boro AK (2002) Electrochemical machining: new possibilities for micromachining. Rob Comput Integr Manuf 18:283–289. doi:10.1016/S0736-5845(02)00019-4
20. Sundarram SS (2008) Development of electrochemical micro-machining. M Sc thesis, Texas A&M University, USA Available on: http://repository.tamu.edu/bitstream/handle/1969.1/86045/Sri.pdf? Accessed 22 Nov 2010
21. Kenney JA, Hwang GS, Shin W (2004) Two-dimensional computational model for electrochemical micromachining with ultrashort voltage pulses. Appl Phys Lett 84(19):3774–3776. doi:10.1063/1.1738937
22. Choi SH, Ryu SH, Choi DK, Chu CN (2007) Fabrication of WC micro-shaft by using electrochemical etching. Int J Adv Manuf Technol 31:682–687. doi:10.1007/s00170-005-0241-4
23. Löwe H, Ehrfeld W, Schiewe J (2002) Micro-electroforming of miniaturized devices for chemical applications. In: Schultze JW, Osaka T, Datta M (eds) Electrochemical microsystems technologies. Taylor & Francis, London, pp 245–268
24. Bhattacharyya B, Malapati M, Munda J (2005) Experimental study on electrochemical micromachining. J Mater Process Technol 169:485–492. doi:10.1016/j.jmatprotec.2005.04.074
25. Wang K, Zhu D, Qu N (2006) Basic research of wire electrochemical micro-machining, International Technology and Innovation Conference. 6-7 Nov, 2006, Hangzhou, China: 1070–1074. http://ieeexplore.ieee.org/stamp/stamp.jsp?arnumber=04752158 Accessed 22 Nov 2010
26. Zhu D, Wang K, Qu NS (2007) Micro wire electrochemical cutting by using in-situ fabricated wire electrode. Ann CIRP 56 (1):241–244. doi:10.1016/j.cirp.2007.05.057